Fermi Arc Criterion for Surface Majorana Modes in Superconducting Time-Reversal Symmetric Weyl Semimetals

Rauf Giwa[1] and Pavan Hosur[1]

[1]*Department of Physics, University of Houston, Texas 77204, USA*

Many clever routes to Majorana fermions have been discovered by exploiting the interplay between superconductivity and band topology in metals and insulators. However, realizations in semimetals remain less explored. We ask, "Under what conditions do superconductor vortices in time-reversal symmetric Weyl semimetals –three-dimensional semimetals with only time-reversal symmetry –trap Majorana fermions on the surface? " If each constant-k_z plane, where z is the vortex axis, contains equal numbers of Weyl nodes of each chirality, we predict a generically gapped vortex and derive a topological invariant $\nu = \pm 1$ in terms of the Fermi arc structure that signals the presence or absence of surface Majorana fermions. In contrast, if certain constant-k_z planes contain a net chirality of Weyl nodes, the vortex is gapless. We analytically calculate ν within a perturbative scheme and provide numerical support with a lattice model. The criteria survive the presence of other bulk and surface bands and yield phase transitions between trivial, gapless and topological vortices upon tilting the vortex. We propose $\mathrm{Li(Fe_{0.91}Co_{0.09})As}$ and $\mathrm{Fe_{1+y}Se_{0.45}Te_{0.55}}$ with broken inversion symmetry as candidates for realizing our proposals.

The interplay of band topology and superconductivity has paved new routes to Majorana fermions (MFs) –as topologically protected zero energy bound states trapped in topological defects such as superconductor vortices [1–20]. Following realizations in semiconductor nanowire-superconductor heterostructures [11, 14, 21], MFs were recently found for the first time in a three-dimensional (3D) system –at the ends of vortices in the bulk superconductor $\mathrm{FeSe_{0.45}Te_{0.55}}$ [22–26]. This inspires a fundamental question: In a 3D superconductor, what properties of the normal state band structure ensure that vortices trap protected MFs at their ends? Restricting to bands with time-reversal symmetry ($\mathcal{T}$), since $\mathcal{T}$ enables a Cooper instability to begin with, sufficient conditions are known in two generic cases: a band insulator (metal) yields MFs if it is topological [5] (a modestly doped topological insulator [6]).

The third type of generic $\mathcal{T}$-preserving band material is a time-reversal symmetric Weyl semimetal (TWSM) [27–30]. Here, point intersections between nondegenerate bands create Weyl nodes (WNs) that possess a chirality of ± 1 and appear in quadruplets to respect $\mathcal{T}$ and Brillouin zone periodicity. Weyl semimetals constitute topological matter as they are immune to perturbations that do not hybridize antichiral WNs, i.e., WNs of opposite chirality and exhibit numerous topological responses [31–57]. On the surface, the bulk band topology manifests as Fermi arcs (FAs) that connect surface projections of antichiral WNs.

Motivated by the quest for MFs, we ask, "What is the fate of a superconductor vortex in a TWSM? " We show that there are three possible vortex phases –(i) gapped, with end-MFs; (ii) gapped, without end MFs; (iii) gapless, with topologically protected chiral MFs dispersing along the vortex axis $\hat{\mathbf{z}}$. Crucially, we prove that the vortex phase relies solely on basic band structure data, namely, the FA configuration on the surface normal to $\hat{\mathbf{z}}$ and the locations of the bulk WNs. Remarkably, simply tilting the vortex can drive transitions between the three phases.

The criteria for the phases are as follows (see Fig. 1). Within each constant-k_z plane, identify the pair(s) of antichiral WNs that are closest to each other in periodic $\boldsymbol{k}$ space. Connect the partners with a geodesic and project it onto the surface. From the remaining WNs, identify the next closest pair(s) and project their geodesic(s) onto the surface, and so on for all WNs and constant-k_z planes. If all the WNs find partners in this process, the surface Brillouin zone will contain a set of lines that, along with the FAs, form closed *Fermi-geodesic loops*. In general, the surface will also carry closed Fermi loops and Dirac nodes. If the total number of Fermi-geodesic loops Fermi loops and Dirac nodes is M, we predict a gapped vortex with a topological invariant

$$\nu = (-1)^M \tag{1}$$

Thus, odd M yields a topologically protected MF in the vortex core on the surface whereas even M does not. All WNs find partners only if each constant-k_z plane contains equal numbers of left- and right-handed WNs. For a minimal TWSM with four WNs at $(\pm\boldsymbol{K}_1, \pm\boldsymbol{K}_2)$, a vortex direction such that $|K_{1z}| = |K_{2z}|$ ensures this, while general TWSMs with more WNs need a mirror or glide symmetry plane parallel to $\hat{\mathbf{z}}$ –which is present in most TWSMs [45, 58–60] – to ensure all WNs are partnered. Generically, though, some WNs will lack partners and the surface will host open *Fermi-geodesic arcs* whose end points will be projections of the unpartnered WNs. Each such WN will contribute a 1D chiral MF to the bulk vortex spectrum with a chirality equal to its own chirality times the vorticity of ± 1. The vortex will be in a gapless phase protected by k_z conservation, analogous to the topological protection of a Weyl semimetal by 3D momentum conservation.

These criteria hold for general pairing symmetries provided the superconductor is gapped in the absence of a vortex. They survive doping around the WNs if the resulting Fermi surfaces are well separated and the presence of trivial Fermi surfaces with rare exceptions. They are also im-

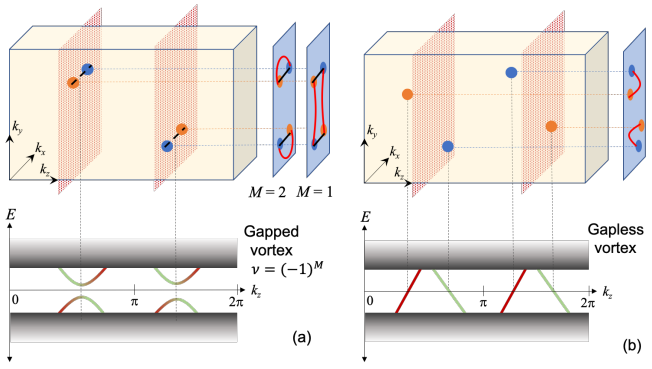

Figure 1. Schematic of the main result. Orange (blue) dots denote right(left)-handed WNs which produce right(left)-moving chiral MFs, colored red (green), inside the vortex. To determine the vortex phase, identify pairs of antichiral WNs at the same k_z and project the line joining them onto the surface. If these lines (solid black), along with the FAs (red curves), form M closed loops, the vortex is gapped and has a topological invariant $\nu = (-1)^M$ (a), whereas open arcs produce a gapless vortex (b).

mune to surface effects unless the surface is exposed to a topological insulator, in which case M effectively acquires the odd number of surface Fermi loops or Dirac nodes of the latter. Finally, Eq. (1) captures the known results for metals [6] and insulators [5], which lack Fermi-geodesic contours but may have Fermi loops and Dirac nodes.

Equation (1) is obtained by computing the $\mathbb{Z}_2$ topological invariant for the vortex viewed as a 1D superconductor [7, 61, 62]. We require a mild assumption in the clean limit: for a given WN, if the two nearest antichiral WNs at the same k_z are at distances ΔK_1 and ΔK_2, then $e^{\frac{\hbar\xi}{\Delta_0}[v_1(\Delta K_1)^2 - v_2(\Delta K_2)^2]} \gg 1$ or $\Delta K_1 \gtrsim \Delta K_2$, where Δ_0 and ξ are superconducting properties –the uniform pairing amplitude and coherence length, respectively –and v_i is the typical Weyl velocity along ΔK_i. This condition ensures that the dominant hybridization is between chiral MFs from neighboring antichiral WNs, assuming hybridization is driven by band curvature. If hybridization is due to nonmagnetic disorder that is smooth over distance ℓ_D, the requirement becomes $\Delta K_1 \gg \ell_D^{-1} \gg \Delta K_2$ while magnetic disorder invalidates Eq. (1). Disorder can be suppressed in principle whereas band curvature is unavoidable, so a physical regime of validity of Eq. (1) exists. We neglect hybridization between equi-chiral chiral MFs, i.e., chiral MFs of the same chirality, which amounts to smoothly deforming any accidentally gapless nonchiral vortex minibands away from zero energy.

Heuristically, Eq. (1) says that vortex-end MFs are present (absent) if the TWSM normal state is "closer" to a topological (trivial) insulator. To see this, imagine moving the WNs along the geodesics and annihilating them in pairs. If all WNs get annihilated, the resulting insulator will be topological (trivial) if the surface FAs evolve into an odd (even) number of surface Fermi loops, while the vortex will be topological (trivial). However, the vortex spectrum remains gapped in the process, so its topological state before and after WN annihilation must be the same.

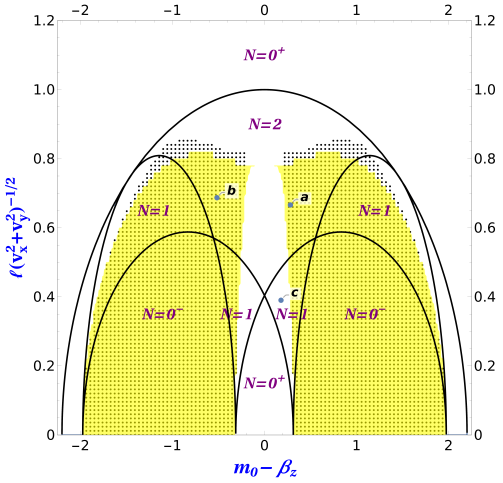

Figure 2. Vortex topological phases predicted by Eq. (1) and computed numerically. The yellow mask (black dots) denote a vortex predicted (computed) to be topological. Black lines separate the normal states: TWSMs with $N = 1, 2$ quadruplets of WNs at $k_z = 0$, trivial ($N = 0^+$) and topological ($N = 0^-$) insulators. We fix $v_{x,y} = 1.18, .856$, $\beta_{x,y,z} = .856, 1.178, 3.0$, $\Delta(r) = 0.42 \tanh(0.3r)$ and $L_{x,y} = 31$. Points **t**, **m** and **b** are further studied in Fig. 3

Recently, Refs. [63, 64] showed that s-wave superconductor vortices in Dirac semimetals can trap helical MFs protected by crystal symmetries. Unlike those vortices, the gapless vortex here is a 1D phase of matter rather than a critical point as it cannot be gapped out by perturbatively changing the crystal space group. Reference [65] found that below a critical doping in a lattice model of a Dirac semimetal with two Dirac nodes, an s-wave vortex normal to the line joining the nodes is gapped and traps a surface MF. The MF survives when the Dirac semimetal is perturbed into a minimal TWSM with four WNs in the plane normal to the vortex, assuming s-wave pairing even with broken inversion symmetry ($\mathcal{I}$) in the TWSM. In comparison, our criteria include the TWSM results of Reference [65] at low doping, but allow arbitrary numbers and configurations of type-I WNs, trivial Fermi surfaces and filled topological bands in the bulk, FAs, Fermi loops and Dirac nodes on the surface, and arbitrary pairing that opens a full gap when uniform.

Continuum analytics:- Consider a canonical WN of chirality $h = \pm 1$ described by $H_W(\boldsymbol{P}) = h \sum_j v_j \Sigma_j P_j - \mu$, where Σ_j, $j = X, Y, Z$, are Pauli matrices spanning the lowest two bands and $\boldsymbol{P}$ is the momentum relative to the WN. At $P_Z = 0$, H_W resembles the 2D surface Hamiltonian of a 3D topological insulator [3, 5, 6, 66]. If $v_X = v_Y$ and $\mu = 0$, it yields a pseudospin-polarized MF with $\langle \Sigma_Z \rangle = w$ in the core of an s-wave superconductor vortex,

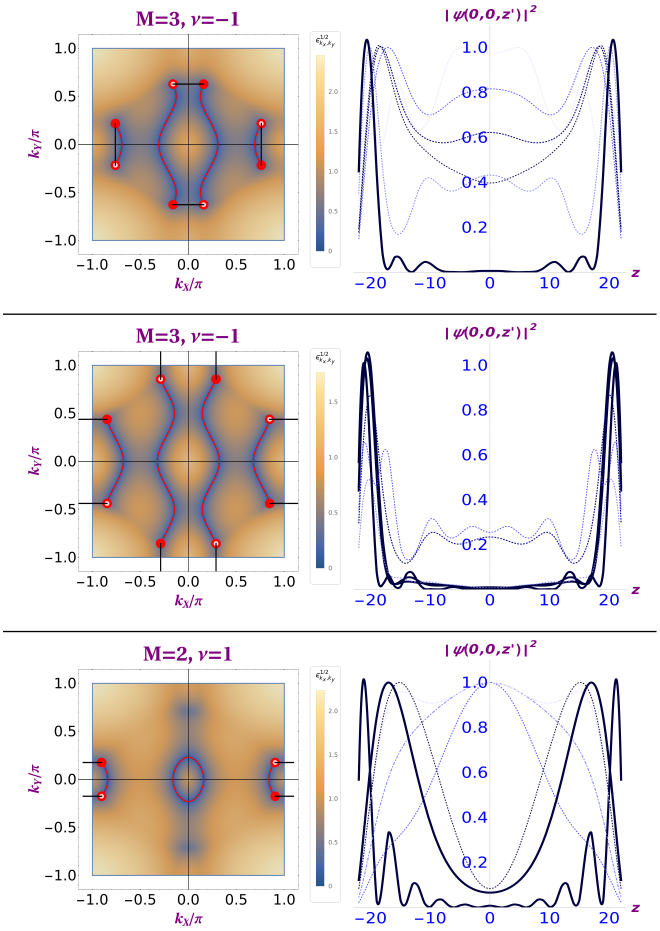

Figure 3. Left column: Color plots of the lowest band for a 45-layer slab in the normal state for the points **t**, **m** and **b** in Fig. 2 defined by $l = 0.942, m_0 = 6.28$ (top), $l = 0.972$, $m_0 = 5.48$ (middle) and $l = 0.552$, $m_0 = 6.18$ (bottom). Red filled (empty) circles denote surface projections of right-(left-)handed WNs. Surface projections of geodesics (black lines) connecting anti-chiral WNs at $k_z = 0$ form M closed loops along with the FAs (red curves). Right column: Probability densities of six lowest energy states along a z-oriented vortex in a $31 \times 31 \times 45$-site system. Bold and dotted lines mark states with energies $E < 5.0 \times 10^{-3}$, considered "zero energy", and $E > 1.0 \times 10^{-2}$.

$\Delta(\boldsymbol{R}) = \Delta(R)e^{iw\Theta}$, $w = \pm 1$ [5]. Being topologically protected, the MF will survive albeit with partial polarization, $0 < w\langle\Sigma_Z\rangle < 1$, when $v_X \neq v_Y$, $\mu \neq 0$ and the pairing is arbitrary but real and nonzero on the Fermi surface. In fact, the MF only requires a Fermi surface Berry phase of π in the weak-pairing, smooth-vortex limit [6]. When $P_Z \neq 0$, the MF disperses as $E_h = hv_Z P_Z \langle\Sigma_z\rangle$, thus realizing a chiral MF with chirality h at $P_Z = 0$ or the k_z of the parent WN. In a real TWSM, k_z conservation forbids hybridization between chiral MFs whose parent WNs are at different k_z, resulting in a gapless vortex[Fig. 1(b)].

Next, consider a minimal TWSM with one quadruplet of WNs at $(\pm\boldsymbol{K}_1, 0)$, $(\pm\boldsymbol{K}_2, 0)$, where WNs at $\pm\boldsymbol{K}_n$

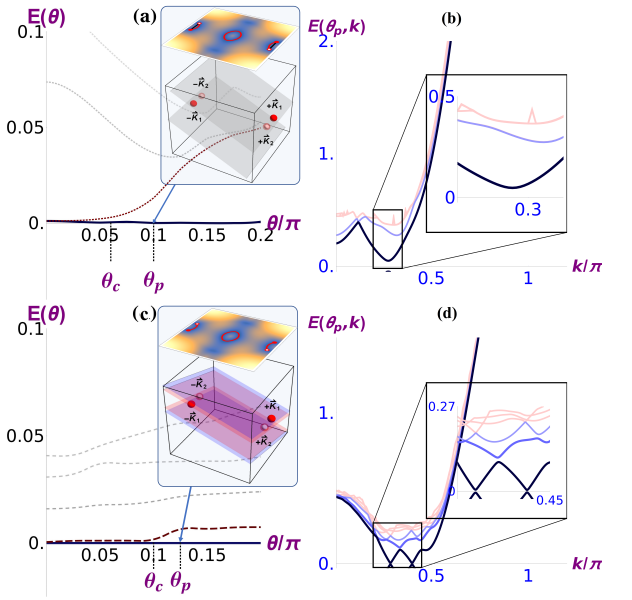

Figure 4. Topological phase transitions upon tilting the $M = 2$ trivial vortex in Fig. 3 (bottom) obtained by diagonalization in real-space (a, c) and k-space (b, d). (a) Tilting about the x-axis produces $M = 3$ (inset) and gaps out one of the two MFs at $\theta_c \approx 0.06\pi$. (b) At $\theta_p = 0.1\pi$, the bulk vortex is gapped, so the surviving MF in (a) at $\theta > \theta_c$ is protected and the vortex is topological. (c, d) Analogous figures for tilting about $x + y = z = 0$. In (c), a small gap opens for one MF at $\theta_c \approx 0.1\pi$ while the surface has open Fermi-geodesic arcs (inset). (d) The bulk vortex is gapless, indicating that the gap in (c) is a finite size gap.

are related by $\mathcal{T}$ and have chirality $(-1)^n$. Suppose FAs on the $z = 0$ surface connect $\boldsymbol{K}_1$ to $\boldsymbol{K}_2$ and $-\boldsymbol{K}_1$ to $-\boldsymbol{K}_2$, and Fermi surfaces around the WNs are well separated. In the presence of a superconductor vortex along $\hat{\mathbf{z}}$, each WN produces a chiral MF dispersing along $(-1)^n\hat{\mathbf{z}}$ with a wavefunction $\psi_{\pm n} = e^{i\boldsymbol{K}_n\cdot\boldsymbol{r}}\varphi_n(\boldsymbol{r})$, where $\varphi_n(\boldsymbol{r})$ is the zero mode of the vortex Hamiltonian near the n^{th} WN. The chiral MFs remain robust when $|\boldsymbol{K}_n\xi| \to \infty$, but hybridize for finite $|\boldsymbol{K}_n\xi|$. Neglecting hybridization between equi-chiral chiral MFs, a generic perturbation H' in the basis $(\psi_{+1}, \psi_{-1}, \psi_{+2}, \psi_{-2})^T$ has the form $H' = \begin{pmatrix} 0 & iQ \\ -iQ^\dagger & 0 \end{pmatrix}$ where $Q = \begin{pmatrix} q_{12} & q_{1\bar{2}} \\ q_{\bar{1}2} & q_{\bar{1}\bar{2}} \end{pmatrix}$ and $q_{mn} = \langle\psi_m|H'|\psi_n\rangle$. If H' preserves $\mathcal{T}$, then $q_{mn} = q_{\bar{m}\bar{n}}$ and the vortex is a gapped 1D superconductor with topological invariant $\nu = \mathrm{sgn}(\mathrm{Pf}[H']) = \mathrm{sgn}(|q_{12}|^2 - |q_{1\bar{2}}|^2)$ [7]. For a spatially smooth perturbation, q_{mn} decays with $|\boldsymbol{K}_m - \boldsymbol{K}_n|$; for instance, band curvature terms yield $q_{mn} \sim e^{-\frac{1}{2}|K_m - K_n|^2\xi/\Delta_0}$ for a linear vortex profile with slope Δ_0/ξ [67]. Then, $|\boldsymbol{K}_1 - \boldsymbol{K}_2| \lesssim |\boldsymbol{K}_1 + \boldsymbol{K}_2|$ produces a trivial vortex while $|\boldsymbol{K}_1 - \boldsymbol{K}_2| \gtrsim |\boldsymbol{K}_1 + \boldsymbol{K}_2|$ yields a topological vortex with end MFs. On the surface, geodesics connecting $\boldsymbol{K}_1$ to $\boldsymbol{K}_2$ and $-\boldsymbol{K}_1$ to $-\boldsymbol{K}_2$, along with the FAs, form $M = 2$ loops. In contrast, geodesics

connecting $\boldsymbol{K}_1$ to $-\boldsymbol{K}_2$ and $-\boldsymbol{K}_1$ to $\boldsymbol{K}_2$ form $M = 1$ loops with the FAs. Thus, there is a one-to-one correspondence between ν and M that is captured by Eq. (1). The Gaussian form of q_{mn} further ensures only logarithmic corrections to the above inequalities due to $\mathcal{O}(1)$ prefactors.

Next, consider moving the WNs away from $k_z = 0$ in pairs while preserving $\mathcal{T}$ in the normal state. If $K_{1z} = K_{2z}$, the chiral MF $\psi_{+1}(\boldsymbol{r})$ can hybridize with $\psi_{+2}(\boldsymbol{r})$ but not with $\psi_{-2}(\boldsymbol{r})$, so the resulting vortex is adiabatically connected to the trivial vortex where all WNs are at $k_z = 0$, $q_{12} \neq 0$ and $q_{1\bar{2}} = 0$. In contrast, if $K_{1z} = -K_{2z}$, the adiabatic equivalent with all WNs at $k_z = 0$ has $q_{1\bar{2}} \neq 0$ and $q_{12} = 0$, which is a topological vortex. These conclusions extend straightforwardly to more quadruplets of WNs, thus proving Eq. (1) for arbitrary configurations of WNs and FAs.

Finally, let us consider the effects of additional bands on our criteria. A filled topological band will produce a 2D Dirac node or Fermi loop on the surface in the normal state, thereby changing the parity of M. However, the superconductor vortex will trap another surface MF and acquire a bulk gap due to this band, thus preserving Eq. (1). Suppose the bulk also contains trivial Fermi surfaces, i.e., Fermi surfaces that do not enclose WNs or other band intersections. For pairing that is real and nonzero on the Fermi surface, a vortex will contain bands $\varepsilon_n(k_z) \sim \frac{\Delta_0}{\xi l_F(k_z)}\left(n + \frac{1}{2} + \frac{\phi_F(k_z)}{2\pi}\right)$ for each trivial Fermi surface, where $n \in \mathbb{Z}$ and $l_F(k_z)$ ($[\phi_F(k_z)]$) is the perimeter (Berry phase) of the Fermi surface cross section at k_z [6]. Unless $\phi_F(k_z) = 0$, trivial Fermi surfaces come in pairs with opposite Berry phases $\pm\phi_F(k_z)$ to ensure that the constant-k_z slice is a sensible 2D metal. As a result, slices with $\phi_F(k_z) \neq \pi$ will acquire a vortex minigap $\sim \Delta_0/\xi l_F(k_z)$ while slices with $\phi_F(k_z) = \pm\pi$, where the minigap vanishes, will host counter propagating chiral MFs that will generically hybridize and gap out. In summary, additional bands will not interconvert gapped and gapless vortices and filled bands always preserve our general criteria.

For gapped vortices, predicted to obey Eq. (1), curable violations due to trivial Fermi surfaces occur in two cases: (i) a surface Fermi loop or Dirac node gets buried under the surface projection of a bulk Fermi surface, resulting in $M_{\text{observable}} = M-1$. This can be cured in principle by doping to expose the relevant surface state; (ii) a Fermi surface centered at $k_z = 0$ or π is past the doping threshold for a vortex phase transition [6], which changes the vortex phase without changing M. This can be fixed by noting that such a Fermi surface has a pair of slices away from $k_z = 0, \pi$ where $\phi_F(k_z) = \pi$. An incurable violation occurs when $\phi_F(k_z) = \pi$ at the precise k_z where a WN exists, the WN is closer to the trivial Fermi surface than to other antichiral WNs at the same k_z *and* the chiral MFs produced by the trivial Fermi surface and the WN have opposite chiralities. Then, H' must include hybridization between these MFs, but Eq. (1) is ruined because M stays unchanged.

Lattice numerics:- We support our general claims with numerics on an orthorhombic lattice model defined by $H(\boldsymbol{k}) = \tau_x \boldsymbol{\sigma} \cdot \boldsymbol{d}(\boldsymbol{k}) + \tau_z m(\boldsymbol{k}) - \tau_y \sigma_z \ell$ where $d_i = v_i \sin k_i$, $i = x, y, z$, $m(\boldsymbol{k}) = m_0 - \sum_i \beta_i \cos k_i$ and τ_i (σ_i) are Pauli matrices in orbital (spin) space. Varying $\beta_{x,y,z}$ and ℓ allows tuning into trivial and topological insulating phases as well as TWSMs with up to two quadruplets of WNs each at $k_z = 0, \pi$ at the Fermi level. We then introduce an s-wave superconductor vortex $\Delta(\boldsymbol{r}) = |\Delta(r)|\, e^{i\theta}$ and diagonalize the Bogoliubov-deGennes Hamiltonian in 2D real space at fixed k_z to obtain the spectrum and the topological invariant [7] for a class D 1D superconductor [61, 62]. In [68], we describe graphical methods for determining the normal state of $H(\boldsymbol{k})$ and FA configuration as well as further details of the lattice numerics. Figure 2 shows that the prediction using Eq. (1) agrees excellently with the explicit calculation. We found smaller mismatch for larger systems or weaker pairing, suggesting that it is due to departure from the thermodynamic and weak-pairing limits.

Figure 3 shows the Fermi-geodesic loops in the normal state and the probability density of the lowest few vortex modes for select points in Fig. 2. The FAs are obtained by plotting the lowest energy at each surface momentum in the normal phase and the geodesics are simply straight lines connecting proximate antichiral WNs at $k_z = 0$. The probability densities are computed by diagonalizing the vortex Hamiltonian in 3D real space. For each selected point, we find that the number of MFs localized to the vortex ends equals M. In Fig. 4, we show that tilting the vortex drives phase transitions between trivial, topological and gapless vortices since geodesics connect WNs at the same k_z. The transitions are expected at infinitesimal tilting in the weak-pairing, smooth-vortex limit, while the numerics find the transitions to occur at small angles.

Candidate material:- We propose Li($Fe_{0.91}Co_{0.09}$)As and $Fe_{1+y}Se_{0.45}Te_{0.55}$ with broken $\mathcal{I}$ as candidate materials. Li($Fe_{0.91}Co_{0.09}$)As is a Dirac semimetal with two Dirac nodes on the c axis of the crystal [69] and shows strong type-II superconductivity below $T_c \approx 9$ K [70]. $FeSe_{0.45}Te_{0.55}$ realizes a doped topological insulator that turns into a type-II superconductor below $T_c \approx 14.5$ K [25, 26], but the normal state also has two Dirac nodes along the c axis ~ 15 meV above the Fermi level that may be accessed with naturally occurring Fe dopants [69]. Perturbatively breaking $\mathcal{I}$ while preserving $\mathcal{T}$ will turn the Dirac semimetals into a TWSM with four WNs at $\pm\boldsymbol{K}_1, \pm\boldsymbol{K}_2$ with $K_1^c \approx K_2^c \gg |\boldsymbol{K}_1 - \boldsymbol{K}_2|$. If superconductivity survives $\mathcal{I}$ breaking, a vortex along $\hat{\mathbf{z}}$ will be topological (trivial) according to Eq. (1) if $|K_{1z}| = |K_{2z}|$ and $(\hat{\mathbf{z}} \times \boldsymbol{K}_1) \cdot (\hat{\mathbf{z}} \times \boldsymbol{K}_2) > 0$ (< 0), whereas a vortex in any other direction will be gapless. Assuming typical values $v \sim 10^5$ m/s for the Dirac velocity, chemical potential $\mu \sim 100$ K relative to the WNs, $\Delta_0 \sim 5$ K, $\xi \sim 5$ nm $\ll$ the penetration depth $d \sim 10^2$ nm ob-

served in LiFeAs [64] which guarantees negligible inter-vortex tunneling ($\propto e^{-d/\xi}$), and $|\boldsymbol{K}_1 - \boldsymbol{K}_2|/K_1^c \approx 0.1$, we estimate a vortex gap of ~ 0.1 K. However, the gap depends exponentially on ξ, $|\boldsymbol{K}_1 - \boldsymbol{K}_2|$ and Δ_0, so it will change substantially for small changes in their values [71].

We acknowledge financial support from NSF-DMR-2047193.

[1] Jason Alicea. New directions in the pursuit of majorana fermions in solid state systems. *Rep. Prog. Phys.*, 75(7), 2012. doi:10.1088/0034-4885/75/7/076501. (document)

[2] Andreas Aste. A direct road to majorana fields. *Symmetry*, 2(4):1776–1809, 2010. ISSN 2073-8994. doi: 10.3390/sym2041776.

[3] C. W. J. Beenakker. Search for majorana fermions in superconductors. *Annu. Rev. Condens. Matter Phys.*, 4(1):113, 2013. doi:10.1146/annurev-conmatphys-030212-184337. (document)

[4] Steven R. Elliott and Marcel Franz. Colloquium: Majorana fermions in nuclear, particle, and solid-state physics. *Rev. Mod. Phys.*, 87(1), 2015. doi:10.1103/revmodphys.87.137.

[5] Liang Fu and C. L. Kane. Superconducting proximity effect and majorana fermions at the surface of a topological insulator. *Phys. Rev. Lett.*, 100(9):96407, 2008. doi: 10.1103/physrevlett.100.096407. (document)

[6] Pavan Hosur, Pouyan Ghaemi, Roger S. K. Mong, and Ashvin Vishwanath. Majorana modes at the ends of superconductor vortices in doped topological insulators. *Physics Reviews Letters*, 107:097001, 2011. doi: 10.1103/physrevlett.107.097001. (document)

[7] A Yu Kitaev. Unpaired majorana fermions in quantum wires. *Phys.-Uspekhi*, 44(10S):131, 2001. doi: 10.1070/1063-7869/44/10s/s29. (document)

[8] Martin Leijnse and Karsten Flensberg. Introduction to topological superconductivity and majorana fermions. *Semicond. Sci. and Technol.*, 27(12), 2012. doi:10.1088/0268-1242/27/12/124003.

[9] Qin Liu, Chen Chen, Tong Zhang, Rui Peng, Ya Jun Yan, Chen Hao Ping Wen, Xia Lou, Yu Long Huang, Jin Peng Tian, Xiao Li Dong, Guang Wei Wang, Wei Cheng Bao, Qiang Hua Wang, Zhi Ping Yin, Zhong Xian Zhao, and Dong Lai Feng. Robust and clean majorana zero mode in the vortex core of high-temperature superconductor $\mathrm{Li}_{0.84}\mathrm{Fe}_{0.16}\mathrm{OHFeSe}$. *Phys. Rev. X*, 8(4):41056, 2018.

[10] Xiao Ping Liu, Yuan Zhou, Yi Fei Wang, and Chang De Gong. Characterizations of topological superconductors: Chern numbers, edge states and majorana zero modes. *New J. Phys.*, 19(9), 2017. doi:10.1088/1367-2630/aa8022.

[11] Roman M. Lutchyn, Tudor D. Stanescu, and S. Das Sarma. Search for majorana fermions in multiband semiconducting nanowires. *Phys. Rev. Lett.*, 106(12):1, 2011. doi: 10.1103/physrevlett.106.127001. (document)

[12] Ning Ma. Majorana fermions in condensed matter: An outlook. *Phys. B: Condens. Matter*, 512:100, 2017. doi: 10.1016/j.physb.2017.01.028.

[13] N. Mohanta and A. Taraphder. Topological superconductivity and majorana bound states at the $\mathrm{LaAlO_3SrTiO_3}$ interface. *Europhys. Lett.*, 108(6), 2014.

[14] V. Mourik, K. Zuo, S. M. Frolov, S. R. Plissard, E. P. A. M. Bakkers, and L. P. Kouwenhoven. Signatures of majorana fermions in hybrid superconductor-semiconductor nanowire devices. *Science*, 336(6084):1003, 2012. doi: 10.1126/science.1222360. (document)

[15] Stevan Nadj-Perge, Ilya K. Drozdov, Jian Li, Hua Chen, Sangjun Jeon, Jungpil Seo, Allan H. MacDonald, B. Andrei Bernevig, and Ali Yazdani. Observation of majorana fermions in ferromagnetic atomic chains on a superconductor. *Science*, 346(6209):602, 2014. doi: 10.1126/science.1259327.

[16] Xiao Liang Qi and Shou Cheng Zhang. Topological insulators and superconductors. *Rev. Mod. Phys.*, 83(4), 2011. doi:10.1103/revmodphys.83.1057.

[17] N. Read and Dmitry Green. Paired states of fermions in two dimensions with breaking of parity and time-reversal symmetries and the fractional quantum hall effect. *Phys. Rev. B*, 2000. doi:10.1103/physrevb.61.10267. (document)

[18] Leonid P. Rokhinson, Xinyu Liu, and Jacek K. Furdyna. The fractional a. c. josephson effect in a semiconductor-superconductor nanowire as a signature of majorana particles. *Nat. Phys.*, 8(11):795, 2012. doi:10.1038/nphys2429.

[19] Masatoshi Sato and Satoshi Fujimoto. Existence of majorana fermions and topological order in nodal superconductors with spin-orbit interactions in external magnetic fields. *Phys. Rev. Lett.*, 105(21):1, 2010. doi: 10.1103/physrevlett.105.217001.

[20] Masatoshi Sato and Yoichi Ando. Topological superconductors: A review. *Rep. Prog. Phys.*, 80(7):1, 2017. doi: 10.1088/1361-6633/aa6ac7. (document)

[21] Tudor D. Stanescu, Jay D. Sau, Roman M. Lutchyn, and S. Das Sarma. Proximity effect at the superconductor-topological insulator interface. *Phys. Rev. B*, 2010. doi: 10.1103/physrevb.81.241310. (document)

[22] Gang Xu, Biao Lian, Peizhe Tang, Xiao-Liang Qi, and Shou-Cheng Zhang. Topological superconductivity on the surface of Fe-based superconductors. *Phys. Rev. Lett.*, 117: 047001, 2016. (document)

[23] T. Machida, Y. Sun, S. Pyon, S. Takeda, Y. Kohsaka, T. Hanaguri, T. Sasagawa, and T. Tamegai. Zero-energy vortex bound state in the superconducting topological surface state of $\mathrm{Fe(Se, Te)}$. *Nat. Mater.*, 18(8):811, 2019.

[24] Lingyuan Kong, Shiyu Zhu, Michał Papaj, Hui Chen, Lu Cao, Hiroki Isobe, Yuqing Xing, Wenyao Liu, Dongfei Wang, Peng Fan, Yujie Sun, Shixuan Du, John Schneeloch, Ruidan Zhong, Genda Gu, Liang Fu, Hong-Jun Gao, and Hong Ding. Half-integer level shift of vortex bound states in an iron-based superconductor. *Nat. Phys.*, 15(11):1181, 2019. doi:10.1038/s41567-019-0630-5.

[25] Dongfei Wang, Lingyuan Kong, Peng Fan, Hui Chen, Shiyu Zhu, Wenyao Liu, Lu Cao, Yujie Sun, Shixuan Du, John Schneeloch, Ruidan Zhong, Genda Gu, Liang Fu, Hong Ding, and Hong-Jun Gao. Evidence for majorana bound states in an iron-based superconductor. *Science*, 2018. doi: 10.1126/science.aao1797. (document)

[26] Peng Zhang, Peng Zhang, Koichiro Yaji, Takahiro Hashimoto, Yuichi Ota, Takeshi Kondo, Kozo Okazaki, Zhijun Wang, Jinsheng Wen, G. D. Gu, Hong Ding, Shik Shin, Peng Zhang, Koichiro Yaji, Takahiro Hashimoto, Yuichi Ota, Takeshi Kondo, Kozo Okazaki, Zhijun Wang, Jinsheng

Wen, G. D. Gu, Hong Ding, and Shik Shin. Observation of topological superconductivity on the surface of an iron-based superconductor. *Science*, 360:182, 2018. doi: 10.1126/science.aan4596. (document)

[27] Conyers Herring. Accidental degeneracy in the energy bands of crystals. *Phys. Rev.*, 52:365, 1937. (document)

[28] G.E. Volovik. *The Universe in A Helium Droplet*. International Series of Monographs on Physics. OUP Oxford, 2009. doi:10.1093/acprof:oso/9780199564842.001.0001.

[29] Xiangang Wan, Ari M. Turner, Ashvin Vishwanath, and Sergey Y. Savrasov. Topological semimetal and fermi-arc surface states in the electronic structure of pyrochlore iridates. *Phys. Rev. B*, 83:205101, 2011. doi: 10.1103/physrevb.83.205101.

[30] N. P. Armitage, E. J. Mele, and Ashvin Vishwanath. Weyl and dirac semimetals in three-dimensional solids. *Rev. Mod. Phys.*, 2018. doi:10.1103/revmodphys.90.015001. (document)

[31] P. Hosur and X. Qi. Recent developments in transport phenomena in weyl semimetals. *C. R. Phys.*, 14(9-10), 2013. doi:10.1016/j.crhy.2013.10.010. (document)

[32] A. A. Burkov. Anomalous hall effect in weyl metals. *Phys. Rev. Lett.*, 113:187202, 2014. ISSN 0031-9007. doi: 10.1103/physrevlett.113.187202.

[33] A A Burkov. Weyl metals. *Annu. Rev. Condens. Matter Phys.*, 9(1):359, 2018. doi:10.1146/annurev-conmatphys-033117-054129.

[34] A A Burkov. Chiral anomaly and transport in weyl metals. *J. Phys.: Condens. Matter*, 27(11):113201, 2015. doi: 10.1088/0953-8984/27/11/113201.

[35] Y. Chen, Si Wu, and A A Burkov. Axion response in weyl semimetals. *Phys. Rev. B*, 88(12):125105, 2013. doi: 10.1103/physrevb.88.125105.

[36] A. A. Zyuzin and A. A. Burkov. Topological response in weyl semimetals and the chiral anomaly. *Phys. Rev. B*, 86 (11):115133, 2012. doi:10.1103/physrevb.86.115133.

[37] P. Hosur and X. L. Qi. Tunable circular dichroism due to the chiral anomaly in weyl semimetals. *Phys. Rev. B*, 91(8), 2015. doi:10.1103/physrevb.91.081106.

[38] Jin Hu, Su-Yang Xu, Ni Ni, and Zhiqiang Mao. Transport of topological semimetals. *Annu. Rev. Mater. Res.*, 49(1): 207, 2019. doi:10.1146/annurev-matsci-070218-010023.

[39] Fernando de Juan, Adolfo G. Grushin, Takahiro Morimoto, and J. E. Moore. Quantized circular photogalvanic effect in weyl semimetals. *Nat. Commun.*, 8(1):15995, 2017. doi: 10.1038/ncomms15995.

[40] Takuro Kobayashi, Taiki Matsushita, Takeshi Mizushima, Atsushi Tsuruta, and Satoshi Fujimoto. Negative thermal magnetoresistivity as a signature of a chiral anomaly in weyl superconductors. *Phys. Rev. Lett.*, 121(20):207002, 2018. doi:10.1103/physrevlett.121.207002.

[41] Karl Landsteiner. Anomalous transport of weyl fermions in weyl semimetals. *Phys. Rev. B*, 89(7):75124, 2014. doi: 10.1103/physrevb.89.075124.

[42] Hailong Li, Haiwen Liu, Hua Jiang, and X. C. Xie. 3d quantum hall effect and a global picture of edge states in weyl semimetals. *Phys. Rev. Lett.*, 125(3):036602, jul 2020. ISSN 0031-9007. doi:10.1103/physrevlett.125.036602.

[43] R. Loganayagam and Piotr Surówka. Anomaly/transport in an ideal weyl gas. *J. High Energy Phys.*, 2012(4):97, 2012. doi:10.1007/jhep04(2012)097.

[44] Naoto Nagaosa, Takahiro Morimoto, and Yoshinori Tokura. Transport, magnetic and optical properties of weyl materials. *Nat. Rev. Mater.*, 5(8):621, 2020. doi:10.1038/s41578-020-0208-y.

[45] Anna Corinna Niemann, Johannes Gooth, Shu Chun Wu, Svenja Bäßler, Philip Sergelius, Ruben Hühne, Bernd Rellinghaus, Chandra Shekhar, Vicky Süß, Marcus Schmidt, Claudia Felser, Binghai Yan, and Kornelius Nielsch. Chiral magnetoresistance in the weyl semimetal nbp. *Sci. Rep.*, 7:3, 2017. doi:10.1038/srep43394. (document)

[46] Pallab Goswami, Girish Sharma, and Sumanta Tewari. Optical activity as a test for dynamic chiral magnetic effect of weyl semimetals. *Phys. Rev. B*, 92(16):161110, 2015. doi: 10.1103/physrevb.92.161110.

[47] Chao-Xing Liu, Peng Ye, and Xiao-Liang Qi. Chiral gauge field and axial anomaly in a weyl semimetal. *Phys. Rev. B*, 87(23):235306, 2013. doi:10.1103/physrevb.87.235306.

[48] K.-Y. Yang, Y.-M. Lu, and Y Ran. Quantum hall effects in a weyl semimetal: Possible application in pyrochlore iridates. *Phys. Rev. B*, 84(7):75129, 2011. doi: 10.1103/physrevb.84.075129.

[49] Chandra Shekhar, Ajaya K. Nayak, Yan Sun, Marcus Schmidt, Michael Nicklas, Inge Leermakers, Uli Zeitler, Yurii Skourski, Jochen Wosnitza, Zhongkai Liu, Yulin Chen, Walter Schnelle, Horst Borrmann, Yuri Grin, Claudia Felser, and Binghai Yan. Extremely large magnetoresistance and ultrahigh mobility in the topological weyl semimetal candidate nbp. *Nat. Phys.*, 11(8):645, 2015. doi: 10.1038/nphys3372.

[50] Kabyashree Sonowal, Ashutosh Singh, and Amit Agarwal. Giant optical activity and kerr effect in type-I and type-II weyl semimetals. *Phys. Rev. B*, 100:085436, 2019.

[51] D T Son and B. Z Spivak. Chiral anomaly and classical negative magnetoresistance of weyl metals. *Phys. Rev. B*, 88(10):104412, 2013. doi:10.1103/physrevb.88.104412.

[52] C. J. Tabert, J. P. Carbotte, and E. J. Nicol. Optical and transport properties in three-dimensional dirac and weyl semimetals. *Phys. Rev. B*, 93(8), 2016. doi: 10.1103/physrevb.93.085426.

[53] M. M. Vazifeh and M. Franz. Electromagnetic response of weyl semimetals. *Phys. Rev. Lett.*, 111(2):27201, 2013. doi: 10.1103/physrevlett.111.027201.

[54] Shuo Wang, Ben Chuan Lin, An Qi Wang, Da Peng Yu, and Zhi Min Liao. Quantum transport in dirac and weyl semimetals: A review. *Advances in Physics: X*, 2(3):518, 2017. doi:10.1080/23746149.2017.1327329.

[55] Huichao Wang and Jian Wang. Electron transport in dirac and weyl semimetals. *Chin. Phys. B*, 27(10):107402, 2018. doi:10.1088/1674-1056/27/10/107402.

[56] Min Lv and Shou-Cheng Zhang. Dielectric function, friedel oscillation and plasmons in weyl semimetals. *Int. J. Mod. Phys. B*, 27(25):1350177, 2013. doi: 10.1142/s0217979213501774.

[57] H. B. Nielsen and M Ninomiya. The adler-bell-jackiw anomaly and weyl fermions in a crystal. *Phys. Lett. B*, 130 (6):389, 1983. doi:10.1016/0370-2693(83)91529-0. (document)

[58] Lijun Meng, Jiafang Wu, Jianxin Zhong, and Rudolf A. Romer. A type of robust superlattice type-I weyl semimetal with four weyl nodes. *Nanoscale*, 11:18358, 2019. (docu-

ment)

[59] Hongming Weng, Chen Fang, Zhong Fang, B. Andrei Bernevig, and Xi Dai. Weyl semimetal phase in noncentrosymmetric transition-metal monophosphides. *Phys. Rev. X*, 5(1):11029, 2015. doi:10.1103/physrevx.5.011029.

[60] Jianpeng Liu and David Vanderbilt. Weyl semimetals from noncentrosymmetric topological insulators. *Phys. Rev. B*, 155316:1, 2014. doi:10.1103/physrevb.90.155316. (document)

[61] Shinsei Ryu, Andreas P. Schnyder, Akira Furusaki, and Andreas W.W. Ludwig. Topological insulators and superconductors: Tenfold way and dimensional hierarchy. *New J. Phys.*, 12:1367, 2010. doi:10.1088/1367-2630/12/6/065010. (document)

[62] Andreas P. Schnyder, Shinsei Ryu, Akira Furusaki, and Andreas W.W. Ludwig. Classification of topological insulators and superconductors. *AIP Conf. Proc.*, 1134:10, 2009. doi: 10.1063/1.3149481. (document)

[63] Elio J. Konig and Piers Coleman. Crystalline-symmetry-protected helical majorana modes in the iron pnictides. *Phys. Rev. Lett.*, 122(20), 2019. doi: 10.1103/physrevlett.122.207001. (document)

[64] Shengshan Qin, Lunhui Hu, Congcong Le, Jinfeng Zeng, Fu-chun Zhang, Chen Fang, and Jiangping Hu. Quasi-1d topological nodal vortex line phase in doped superconducting 3d dirac semimetals. *Phys. Rev. Lett.*, 123:027003, 2019. doi:10.1103/physrevlett.123.027003. (document)

[65] Zhongbo Yan, Zhigang Wu, and Wen Huang. Vortex end majorana zero modes in superconducting dirac and weyl semimetals. *Phys. Rev. Lett.*, 124:257001, 2020. doi: 10.1103/physrevlett.124.257001. (document)

[66] A. A. Burkov and Leon Balents. Weyl semimetal in a topological insulator multilayer. *Phys. Rev. Lett.*, 107(12):1, 2011. doi:10.1103/physrevlett.107.127205. (document)

[67] See supplemental material at http://link.aps.org/supplemental for hybridization of chiral majorana fermions which includes refs. [5, 6, 17], . (document)

[68] See supplemental material at http://link.aps.org/supplemental for graphical methods for determining the normal state which includes refs. [72], . (document)

[69] Peng Zhang, Zhijun Wang, Xianxin Wu, Koichiro Yaji, Yukiaki Ishida, Yoshimitsu Kohama, Guangyang Dai, Yue Sun, Cedric Bareille, Kenta Kuroda, Takeshi Kondo, Kozo Okazaki, Koichi Kindo, Xiancheng Wang, Changqing Jin, Jiangping Hu, Ronny Thomale, Kazuki Sumida, Shilong Wu, Koji Miyamoto, Taichi Okuda, Hong Ding, G. D. Gu, Tsuyoshi Tamegai, Takuto Kawakami, Masatoshi Sato, and Shik Shin. Multiple topological states in iron-based superconductors. *Nat. Phys.*, 15(1):41, 2019. (document)

[70] Y. M. Dai, H. Miao, L. Y. Xing, X. C. Wang, P. S. Wang, H. Xiao, T. Qian, P. Richard, X. G. Qiu, W. Yu, C. Q. Jin, Z. Wang, P. D. Johnson, C. C. Homes, and H. Ding. Spin-fluctuation-induced non-fermi-liquid behavior with suppressed superconductivity in $\mathrm{LiFe}_{1-x}\mathrm{Co}_x\mathrm{As}$. *Phys. Rev. X*, 5:031035, 2015. (document)

[71] See supplemental material at http://link.aps.org/supplemental for hybridization gap and topological invariant in the continuum limit which includes refs. [7], . (document)

[72] Liang Fu, C. L. Kane, and E. J Mele. Topological insulators in three dimensions. *Phys. Rev. Lett.*, 98(10):106803, 2007. doi:10.1103/physrevlett.98.106803. (document)

Supplementary material for "Fermi arc criterion for surface Majorana modes in superconducting time-reversal symmetric Weyl semimetals"

Rauf Giwa, Pavan Hosur[1]

[1]*Department of Physics, University of Houston, Houston 77204, USA*

Appendix A: Orthorhombic lattice model of a T-WSM

In this section, we analyze the orthorhombic lattice model studied in the main text and describe how to determine its topological nature in the normal state. To recapitulate, the Bloch Hamiltonian is

$$H(\boldsymbol{k}) = \tau_x \boldsymbol{\sigma} \cdot \boldsymbol{d}\left(\boldsymbol{k}\right) + \tau_z m\left(\boldsymbol{k}\right) - \tau_y \sigma_z \ell - \mu \tag{A1}$$

where $d_i = v_i \sin k_i$, $i = x, y, z$, $m(\boldsymbol{k}) = m_0 - \sum_i \beta_i \cos k_i$ and τ_i and σ_i are Pauli matrices acting on orbital and spin space, respectively. $H(\boldsymbol{k})$ preserves time-reversal ($\mathcal{T} = i\sigma_y \mathbb{K}$), reflection about the xz and yz planes ($M_{i\to -i} = \tau_z \sigma_i$, $i = x, y, z$) and twofold rotation about the z-axis ($R_i = \sigma_i$), but breaks inversion ($\mathcal{I} = \tau_z$), reflection about the xy plane, and twofold rotation about the x and the y axes are broken. Its spectrum is given by

$$\left(E(\boldsymbol{k}) + \mu\right)^2 = v_z^2 \sin k_z^2 + m^2(\boldsymbol{k}) + \left(\sqrt{v_x^2 \sin k_x^2 + v_y^2 \sin k_y^2} \pm \ell\right)^2 \tag{A2}$$

Defining $X = \cos k_x$, $Y = \cos k_y$, a quadruplet of Weyl nodes (WNs) appears in the $k_z = 0$ or π plane at $(K_x, K_y) = (\pm \cos^{-1} X, \pm \cos^{-1} Y)$ for each intersection between the following ellipse and lines within the unit square $X \in [-1, 1]$, $Y \in [-1, 1]$

$$v_x^2 X^2 + v_y^2 Y^2 = v_x^2 + v_y^2 - \ell^2 \tag{A3}$$

$$\beta_x X + \beta_y Y = M_{k_z} = m_0 - \beta_z \cos k_z \tag{A4}$$

When the ellipse and line do not intersect within the unit square, the system is an $\mathcal{T}$-symmetric insulator. These behaviors are depicted in the top panel of Fig. 1

At $\ell = 0$, $\mathcal{I}$ is restored, the system is necessarily insulating since the ellipse circumscribes the unit square and the topological nature of the insulator can be deduced from the parity criterion which only depends on $\mathrm{sgn}[m(\boldsymbol{k})]$ at the eight time-reversal invariant momenta $(0/\pi, 0/\pi, 0/\pi)$. For larger ℓ, the strong topological index of an insulating state can be obtained easily by observing the connectivity of the Fermi arcs on an xy-surface, as shown in the bottom panel of Fig. 1. Imagine tuning a parameter that creates and subsequently annihilates a quadruplet of WNs. Now, nodes are always created as well as annihilated in pairs of opposite chirality. Moreover, creating a pair of nodes and moving them apart leaves behind a surface Fermi arc that connects the surface projections of the nodes. If the nodes switch partners between creation and annihilation – in other words, if a given right-handed WN is created along with a left-handed WN but annihilates a different left-handed WN – a non-degenerate, $\mathcal{T}$-invariant Fermi surface is left behind on the surface. Such a Fermi surface can be viewed as the surface state of a topological insulator doped away from charge neutrality. Therefore, each time WNs switch partners between creation and annihilation, the strong topological index of the bulk insulator toggles.

In the main paper, we choose parameters such that the line defined by $m(k_z = \pi) = 0$ never intersects the ellipse. Then, all the normal state phase transitions occur via crossings in the $k_z = 0$ plane, which gives access to trivial and topological insulators as well as T-WSMs with $N = 1, 2$.

Appendix B: Vortex topological invariant in a minimal lattice model

In this section, we use a perturbative scheme to explicitly determine the topological state of the vortex in the lattice model (A1) in the range of parameters which gives $N = 1$ quadruplet of WNs.

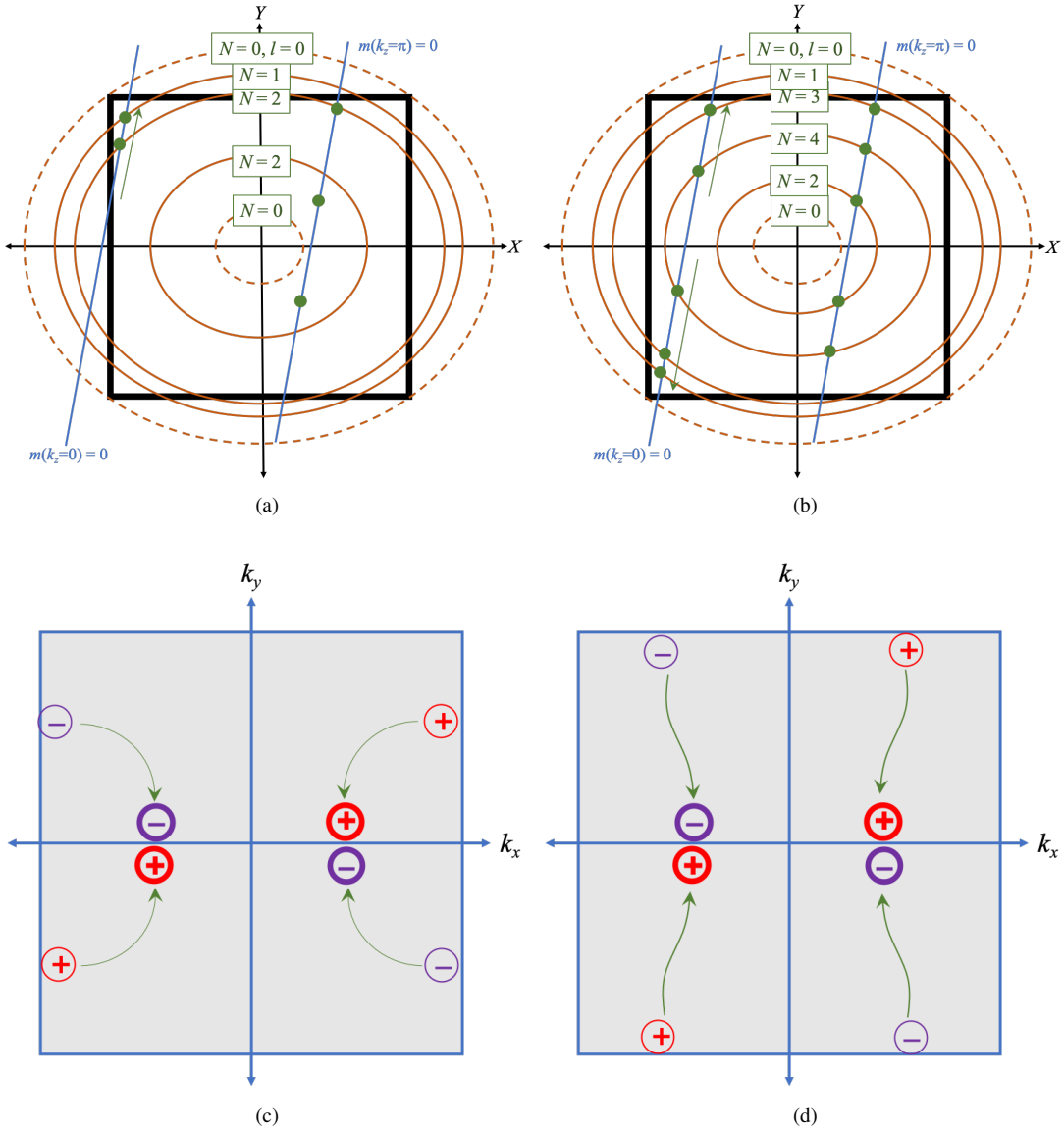

Figure 1. Prescription to determine the number of WN quadruplets (N), the Fermi arc structure on the surface and the $\mathbb{Z}_2$ invariant in the insulating phase in the lattice model (A1). Top: $X = \cos k_z$, $Y = \cos k_y$ and the ellipses and lines are given by (A3) and (A4), respectively, with smaller $|\ell|$ defining larger ellipses. Each ellipse-line intersection within the defines a quadruplet of WNs in the plane defining the line. Green arrows indicate the path of the intersections as the ellipse is enlarged. Solid (dashed) ellipses denote T-WSMs with N quadruplets (insulators with $N = 0$). The $\ell = 0$ ellipse circumscribes the square and defines an $\mathcal{I}$-preserving insulator with $\mathbb{Z}_2$ indices given by the parity criterion [2]. It has the opposite (same) strong index as the innermost ellipse if exactly one line (no or both lines) intersects a vertical and a horizontal edge of the unit square, as shown on the left (right). Bottom: Brillouin zone of the (001) surface and the effect of moving WNs along the paths indicated in the top panel on the Fermi arcs. For simplicity, only the effect of WNs in the $k_z = 0$ plane is shown; the effects of $k_z = \pi$ WNs are identical. Circles with $\pm$ denote the surface projections of right/left-handed WNs, and their trajectories as the ellipse in the top panel is enlarged are indicated by green arrows. These trajectories trace out the Fermi arcs. If a quadruplet is created at a $k_x = -k_x$ plane and annihilated on a $k_y = -k_y$ plane or vice-versa, the Fermi arcs close into a single Fermi surface, implying a change of the bulk strong $\mathbb{Z}_2$ topological index. If a quadruplet is created and destroyed on a $k_x = -k_x$ (or $k_y = -k_y$) plane, the $\mathbb{Z}_2$ invariants corresponding to the ellipse shrunk to a point and the ellipse circumscribing the unit square are the same.

1. Reduction to a canonical Weyl Hamiltonian

We begin with the Bloch Hamiltonian (A1) and assume the parameters are chosen so that there is a single quadruplet of WNs, at $(\pm K_x, \pm K_y, 0)$. The Bloch Hamiltonian at these points has a higher symmetry, namely, $[H(\boldsymbol{K}), \tau_y\sigma_z] = 0$, so it is convenient to work in the eigenbasis of $\tau_y\sigma_z$. For convenience, let us perform a rotation

$$H'(\boldsymbol{K}) = e^{i\tau_x\pi/4} H(\boldsymbol{K}) e^{-i\tau_x\pi/4} = \tau_x \boldsymbol{\sigma}\cdot\boldsymbol{d}(\boldsymbol{k}) + \tau_z\sigma_z\ell - \mu \tag{B1}$$

which explicitly diagonalizes the term proportional to ℓ. Since $|\boldsymbol{d}(\boldsymbol{K})|^2 = \ell^2$ at the nodes according to Eq. (4) of the main paper, the four states at each WN have energies $2\ell, 0, 0, -2\ell$. The two zero energy states explicitly are

$$|A'\rangle = \frac{1}{\sqrt{2}}\left(1,0,0,-e^{i\theta_d}\right)^T \ , \ |B'\rangle = \frac{1}{\sqrt{2}}\left(0,e^{i\theta_d},1,0\right)^T \tag{B2}$$

where $\theta_d = \arg(d_x + id_y)$ and the primes serve as reminders that we have performed a $e^{i\tau_x\pi/4}$ rotation. The low energy Hamiltonian near the WN in the $(|A'\rangle, |B'\rangle)^T$ basis is given by

$$H'_W(\boldsymbol{p}) = (\Sigma_x,\Sigma_y,\Sigma_z)\begin{pmatrix} 0 & 0 & v_z \\ \beta_x \sin K_x & \beta_y \sin K_y & 0 \\ -v_x^2\ell^{-1}\sin K_x\cos K_x & -v_y^2\ell^{-1}\sin K_y\cos K_y & 0 \end{pmatrix}\begin{pmatrix} p_x \\ p_y \\ p_z \end{pmatrix} - \mu \tag{B3}$$

where Σ_i are Pauli operators in the $|A'\rangle, |B'\rangle$ basis. Note that reversing K_J to get to a different WN is equivalent to reversing p_J in H'_W. At $p_z = 0$, H'_W contains only Σ_z and Σ_y. For convenience, we rotate $\Sigma_z \to -\Sigma_x$, $\Sigma_x \to \Sigma_z$ to define $H''_W = e^{i\Sigma_y\pi/4} H'_W e^{-i\Sigma_y\pi/4}$. H''_W in the $p_z = 0$ plane is

$$H''_W(p_z = 0) = \ell^{-1}(\Sigma_x,\Sigma_y)\hat{M}\begin{pmatrix} p_x \\ p_y \end{pmatrix} - \mu \tag{B4}$$

where $\hat{M} = \begin{pmatrix} v_x^2\ell^{-1}\sin K_x\cos K_x & v_y^2\ell^{-1}\sin K_y\cos K_y \\ \beta_x \sin K_x & \beta_y \sin K_y \end{pmatrix}$. To bring this into a canonical form, we perform a singular value decomposition of $\hat{M}$

$$\hat{M} = R(\phi_\Sigma)\begin{pmatrix} v_X & 0 \\ 0 & v_Y \end{pmatrix} R^T(\phi_p) \tag{B5}$$

where $R(\phi) = \begin{pmatrix} \cos\phi & -\sin\phi \\ \sin\phi & \cos\phi \end{pmatrix}$ and $v_{X,Y} > 0$. We have assumed that the WNs at $\pm(K_x, K_y)$ can be brought into a canonical form by proper rotations. This automatically means that the nodes at $\pm(K_x, -K_y)$ need improper rotations. The necessity of singular value decomposition indicates that the principal axes for $\boldsymbol{p}$ and $\boldsymbol{\Sigma}$ are different, and both differ from the Cartesian axes of the original problem. Moreover, $v_X \neq v_Y$, implying that the WN is anisotropic. Nonetheless, this can be brought into a canonical form $H''_W = v_X\Sigma_X P_X + v_Y\Sigma_Y P_Y - \mu$ through the rotations

$$\begin{pmatrix} P_X \\ P_Y \end{pmatrix} = R^T(\phi_p)\begin{pmatrix} p_x \\ p_y \end{pmatrix} \tag{B6}$$

$$\begin{pmatrix} X \\ Y \end{pmatrix} = R^T(\phi_p)\begin{pmatrix} x \\ y \end{pmatrix} \tag{B7}$$

$$\begin{pmatrix} \Sigma_X \\ \Sigma_Y \end{pmatrix} = R^T(\phi_\Sigma)\begin{pmatrix} \Sigma_x \\ \Sigma_y \end{pmatrix} = e^{-i\Sigma_z\phi_\Sigma/2}\begin{pmatrix} \Sigma_x \\ \Sigma_y \end{pmatrix} e^{i\Sigma_z\phi_\Sigma/2} \tag{B8}$$

2. Vortex modes of anisotropic vortex

In the presence of s-wave superconductivity, the Bogoliubov-deGennes Hamiltonian is given by

$$H''_{BdG}(\boldsymbol{P}) = \begin{pmatrix} H''_W(\boldsymbol{P}) & \Delta(\boldsymbol{R}) \\ \Delta^*(\boldsymbol{R}) & -H''_W(\boldsymbol{P}) \end{pmatrix} \tag{B9}$$

in the basis $\frac{1}{\sqrt{2}}\left(c_{A'} + c_{B'}, -c_{A'} + c_{B'}, -c^\dagger_{A'} + c^\dagger_{B'}, -c^\dagger_{A'} - c^\dagger_{B'}\right)^T$. Furthermore, if the superconductivity develops a vortex $\Delta(\boldsymbol{r}) = \Delta_0(r)e^{i\theta}$, where $\theta = \arg(x + iy)$, the pairing term in H''_{BdG} becomes $\Delta(\boldsymbol{R}) = e^{i(\phi_\Sigma + \Theta)}\Delta_0(R)$, where

$\Theta = \arg(X + iY)$. If $v_X = v_Y$, the problem has a rotational symmetry which can be used to obtain the eigenmodes of H''_{BdG} analytically. This result is well-known [1, 3, 5]. When $v_X \neq v_Y$, we can still obtain the eigenmodes analytically in the linear approximation $\Delta_0(R) = \Delta_0 R/\xi$, where ξ is the superconducting coherence length.

We explicitly write

$$H''_{BdG}(\boldsymbol{P}) = \Pi_z H''_W(\boldsymbol{P}) + \frac{\Delta_0 R}{\xi}\left(\Pi_x \cos\left(\Theta + \phi_\Sigma\right) - \Pi_y \sin\left(\Theta + \phi_\Sigma\right)\right) \tag{B10}$$

The ϕ_Σ-dependence can be eliminated by a Π_z-rotation:

$$H'''_{BdG}(\boldsymbol{P}) = e^{-i\Pi_z\phi_\Sigma/2} H''(\boldsymbol{P}) e^{i\Pi_z\phi_\Sigma/2} \tag{B11}$$

$$= \Pi_z H''_W(\boldsymbol{P}) + \frac{\Delta_0}{\xi}\left(\Pi_x X - \Pi_y Y\right) \tag{B12}$$

At $\mu = 0$, we can separate the X and Y parts of the problem via another rotation. Specifically, define

$$H''''_{BdG}(\boldsymbol{P}) = e^{i\Pi_y\Sigma_Y\pi/4} H'''_{BdG}\left(\boldsymbol{P}\right) e^{-i\Pi_y\Sigma_Y\pi/4} \tag{B13}$$

$$= \Pi_z\left(v_X\Sigma_X P_X + \frac{\Delta_0}{\xi}\Sigma_Y X\right) - \left(\Pi_x v_Y P_Y + \Pi_y \frac{\Delta_0}{\xi} Y\right) \tag{B14}$$

$$= \sqrt{\frac{2\Delta_0}{\xi}}\begin{pmatrix} & -i\sqrt{v_X}a_X & i\sqrt{v_Y}a_Y & \\ i\sqrt{v_X}a_X^\dagger & & & i\sqrt{v_Y}a_Y \\ -i\sqrt{v_Y}a_Y^\dagger & & & i\sqrt{v_X}a_X \\ & -i\sqrt{v_Y}a_Y^\dagger & -i\sqrt{v_X}a_X^\dagger & \end{pmatrix} \tag{B15}$$

where $a_J = \sqrt{\frac{\xi}{2\Delta_0 v_J}}\left(\frac{\Delta_0}{\xi}J + iv_J P_J\right), J = X, Y$ is the usual annihilation operator for a quantum harmonic oscillator. The eigenstates of H''''_{BdG} are of the form $\left(|n_X - 1, n_Y - 1\rangle, |n_X, n_Y - 1\rangle, |n_X - 1, n_Y\rangle, |n_X, n_Y\rangle\right)^T$. In this basis,

$$H''''_{BdG}(n_X, n_Y) = \sqrt{\frac{2\Delta_0}{\xi}}\begin{pmatrix} & -i\sqrt{v_X n_X} & i\sqrt{v_Y n_Y} & \\ i\sqrt{v_X n_X} & & & i\sqrt{v_Y n_Y} \\ -i\sqrt{v_Y n_Y} & & & i\sqrt{v_X n_X} \\ & -i\sqrt{v_Y n_Y} & -i\sqrt{v_X n_X} & \end{pmatrix} \tag{B16}$$

$$= \sqrt{\frac{2\Delta_0}{\xi}}\left(\Pi_z\Sigma_Y\sqrt{v_X n_X} + \Pi_x\sqrt{v_Y n_Y}\right) \tag{B17}$$

Thus, it has the spectrum

$$E\left(n_X, n_Y\right) = \pm\sqrt{\frac{2\Delta_0}{\xi}\left(v_X n_X + v_Y n_Y\right)} \tag{B18}$$

In particular, the zero mode is given by $n_X = n_Y = 0$ and has the wavefunction

$$\varphi''''(\boldsymbol{R}) = (0, 0, 0, |0, 0\rangle)^T \equiv (0, 0, 0, 1)^T f_{00}(X, Y) \tag{B19}$$

where $f_{00}\left(X, Y\right) = \sqrt{\frac{\Delta_0}{\pi\xi\sqrt{v_x v_y}}}\exp\left[-\frac{\Delta_0}{2\xi}\left(\frac{X^2}{v_X} + \frac{Y^2}{v_Y}\right)\right]$ is the wavefunction for the $(n_X = 0, n_Y = 0)$ mode of the 2D harmonic oscillator. Undoing the rotations generated by $\Pi_y\Sigma_Y$, Π_z, Σ_y and the singular value decomposition gives

$$\varphi'(\boldsymbol{R}) = e^{-i\Sigma_y\pi/4} e^{i\Pi_z\Sigma_z\phi_\Sigma/2}\varphi'' = \frac{1}{\sqrt{2}} e^{-i\Sigma_y\pi/4}\left(ie^{i\phi_\Sigma}, 0, 0, 1\right)^T f_{00}(X, Y) \tag{B20}$$

$$\varphi'(x, y) = \frac{1}{2}\left(ie^{i\phi_\Sigma}, ie^{i\phi_\Sigma}, -1, 1\right)^T \tilde{f}(x, y) \tag{B21}$$

in the basis $(c_A, c_B, c_B^\dagger, -c_A^\dagger)$, where $\tilde{f}(x, y) = \sqrt{\frac{\Delta_0}{\pi\xi\sqrt{v_X v_Y}}}\exp\left[-\frac{\Delta_0 r^2}{4\xi}\left\{\left(\frac{1}{v_X} + \frac{1}{v_Y}\right) + \left(\frac{1}{v_X} - \frac{1}{v_Y}\right)\cos[2(\theta + \phi_p)]\right\}\right] \equiv \sqrt{\frac{\Delta_0}{\pi\xi\sqrt{v_X v_Y}}}\exp\left[-\frac{\Delta_0 r^2}{4\xi}\left\{\frac{1}{v_+} + \frac{1}{v_-}\cos[2(\theta + \phi_p)]\right\}\right]$. φ' is an eigenstate of charge conjugation: $\mathbb{C}\varphi' \equiv \Pi_y\Sigma_y\varphi'^* = ie^{-i\phi_\Sigma}\varphi'$ and hence, represents a Majorana mode. In the original basis $\left(c_{s\uparrow}, c_{s_\downarrow}, c_{p\uparrow}, c_{p\downarrow}, c_{s\downarrow}^\dagger, -c_{s\uparrow}^\dagger, c_{p\downarrow}^\dagger, -c_{p\uparrow}^\dagger\right)^T$,

$$\varphi(x, y) = \frac{e^{-i\pi/4}}{2\sqrt{2}}\left(-e^{i\phi_\Sigma}, ie^{i(\theta_d + \phi_\Sigma)}, -e^{i\phi_\Sigma}, -ie^{i(\theta_d + \phi_\Sigma)}, -ie^{-i\theta_d}, 1, ie^{-i\theta_d}, 1\right)^T \tilde{f}(x, y) \tag{B22}$$

$$\equiv \chi\tilde{f}(x, y)$$

Finally, $\chi^\dagger\Pi_z\tau_x\sigma_z\chi = 1$, so non-zero k_z induces a dispersion $E(k_z) = v_z \sin k_z$ and thus produces a CMM.

3. Hybridization between CMMs

The Majorana fermions coming from WNs at $(K_x, -K_y)$, $(-K_x, -K_y)$ and $(-K_x, K_y)$ can be obtained by applying the symmetry operations $S_y = i\mathcal{T}M_y = \tau_z\mathbb{K}\otimes y \to -y$, $S_{xy} = -i\Pi_z M_x M_y = \Pi_z\sigma_z \otimes (x,y) \to -(x,y)$ and $S_x = \Pi_z\mathcal{T}M_x = \Pi_z\tau_z\sigma_z\mathbb{K}\otimes x \to -x$, respectively. The result after reinstating the fast spatial variation is

$$\psi_{\lambda_x\lambda_y}(x,y) = \frac{1}{2\sqrt{2}}e^{i(\lambda_x K_x x + \lambda_y K_y y - \lambda_x\lambda_y\pi/4)}\sqrt{\frac{\Delta_0}{\pi\xi\sqrt{v_X v_Y}}}\exp\left[-\frac{\Delta_0 r^2}{4\xi}\left\{\frac{1}{v_+}+\frac{\cos[2(\theta-\lambda_x\lambda_y\phi_p)]}{v_-}\right\}\right]\times$$
$$\left(-e^{i\lambda_x\lambda_y\phi_\Sigma}, i\lambda_y e^{i\lambda_x\lambda_y(\theta_d+\phi_\Sigma)}, -\lambda_x\lambda_y e^{i\lambda_x\lambda_y\phi_\Sigma}, -i\lambda_x e^{i\lambda_x\lambda_y(\theta_d+\phi_\Sigma)}, -i\lambda_y e^{-i\lambda_x\lambda_y\theta_d}, 1, i\lambda_x e^{-i\lambda_x\lambda_y\theta_d}, \lambda_x\lambda_y\right)^T$$

where $\lambda_x = \pm$, $\lambda_y = \pm$. For $K_{x,y}\xi \gg 1$, the leading perturbation from band curvature is given by the matrix elements

$$\left\langle \psi_{\lambda'_x\lambda'_y}\left|H_2\right|\psi_{\lambda_x\lambda_y}\right\rangle = e^{i\pi/4(\lambda'_x\lambda'_y-\lambda_x\lambda_y)}\int_{x,y} e^{i[(\lambda_x-\lambda'_x)K_x x+(\lambda_y-\lambda'_y)K_y y]}\varphi^\dagger_{\lambda'_x\lambda'_y}(x,y)\times$$
$$\frac{1}{2}\left(p_x^2\partial^2_{k_x}H_{BdG}(\lambda_x K_x,\lambda_y K_y)+p_y^2\partial^2_{k_y}H_{BdG}(\lambda_x K_x,\lambda_y K_y)\right)\varphi_{\lambda_x\lambda_y}(x,y) \tag{B23}$$
$$= -\frac{1}{2}e^{i\pi/4(\lambda'_x\lambda'_y-\lambda_x\lambda_y)}\int_{x,y} e^{i[(\lambda_x-\lambda'_x)K_x x+(\lambda_y-\lambda'_y)K_y y]}\varphi^\dagger_{\lambda'_x\lambda'_y}(x,y)\Pi_z\times$$
$$\begin{bmatrix} p_x^2\left(\frac{\lambda_x+\lambda'_x}{2}\tau_x\sigma_x v_x\sin K_x-\tau_z\beta_x\cos K_x\right)+ \\ p_y^2\left(\frac{\lambda_y+\lambda'_y}{2}\tau_x\sigma_y v_y\sin K_y-\tau_z\beta_y\cos K_y\right)\end{bmatrix}\varphi_{\lambda_x\lambda_y}(x,y) \tag{B24}$$

which consists of straightforward Gaussian integrals. First, let us compute the spinor products. In the basis $(|\chi_{++}\rangle, |\chi_{--}\rangle, |\chi_{-+}\rangle, |\chi_{+-}\rangle)$, we find

$$(\lambda_i+\lambda_{i'})\Pi_z\tau_x\sigma_i \to 0; i = x,y \tag{B25}$$

$$\Pi_z\tau_z \to \begin{pmatrix} & & e^{-i\phi_\Sigma}\cos\theta_d\sin(\phi_\Sigma+\theta_d) & -e^{-i\phi_\Sigma}\cos(\phi_\Sigma+\theta_d)\sin\theta_d \\ & 0 & -e^{-i\phi_\Sigma}\cos(\phi_\Sigma+\theta_d)\sin\theta_d & e^{-i\phi_\Sigma}\cos\theta_d\sin(\phi_\Sigma+\theta_d) \\ 0 & & & \end{pmatrix}+ \tag{B26}$$
$$\begin{pmatrix} & & & 0 \\ & & 0 & \\ & & & \\ e^{i\phi_\Sigma}\cos\theta_d\sin(\phi_\Sigma+\theta_d) & -e^{i\phi_\Sigma}\cos(\phi_\Sigma+\theta_d)\sin\theta_d & & \\ -e^{i\phi_\Sigma}\cos(\phi_\Sigma+\theta_d)\sin\theta_d & e^{i\phi_\Sigma}\cos\theta_d\sin(\phi_\Sigma+\theta_d) & & \end{pmatrix}$$

Note that only CMMs coming from nodes of opposite chiralities mix, in which case $\lambda'_x\lambda'_y = -\lambda_x\lambda_y$, and the hybridization is caused by the "mass" term, not the "kinetic" terms, of the Dirac Hamiltonian (A1). Finally, we get the effective Hamiltonian in the basis $\left(|\psi_{++}\rangle, |\psi_{--}\rangle, e^{-i\phi_\Sigma}|\psi_{-+}\rangle, e^{-i\phi_\Sigma}|\psi_{+-}\rangle\right)^T$ as

$$H_{eff} = i\begin{pmatrix} & & q_x & q_y \\ & & q_y & q_x \\ -q_x & -q_y & & \\ -q_y & -q_x & & \end{pmatrix} \tag{B27}$$

where q_i decays as a Gaussian as a function of $\Delta K_i = K_i - (-K_i)$. Explicitly,

$$q_x = \frac{(\Delta K_x)^2 \cos\theta_d \sin(\phi_\Sigma + \theta_d)}{2} \exp\left[-\frac{\xi(\Delta K_x)^2}{2\Delta_0\left(\frac{1}{v_+} + \frac{\cos 2\phi_p}{v_-}\right)}\right] \times \left(\mathbb{V}_+^2\left(\frac{1}{v_+} - \frac{\cos 2\phi_p}{v_-}\right)^2 \beta_x \cos K_x + \mathbb{V}_-^2 \frac{\sin^2 2\phi_p}{v_-^2}\beta_y \cos K_y\right) \tag{B28}$$

$$q_y = -\frac{(\Delta K_y)^2 \cos(\phi_\Sigma + \theta_d) \sin\theta_d}{2} \exp\left[-\frac{\xi(\Delta K_y)^2}{2\Delta_0\left(\frac{1}{v_+} - \frac{\cos 2\phi_p}{v_-}\right)}\right] \times \left(\mathbb{V}_+^2 \frac{\sin^2 2\phi_p}{v_-^2}\beta_x \cos K_x + \mathbb{V}_-^2\left(\frac{1}{v_+} + \frac{\cos 2\phi_p}{v_-}\right)^2 \beta_y \cos K_y\right) \tag{B29}$$

to leading order in $\Delta_0\xi/(\Delta K_x)^2$ and $\Delta_0\xi/(\Delta K_y)^2$, where $\mathbb{V}_\pm^2 = (v_X v_Y)^{-1/2}\left(\frac{1}{v_+} \pm \frac{\cos 2\phi_p}{v_-}\right)^{-1/2}\left(\frac{1}{v_+} \mp \frac{\cos 2\phi_p}{v_-}\right)^{-5/2}$ has units of velocity-squared. For $|\Delta K_x| \gg |\Delta K_y|$ and $|\Delta K_x| \ll |\Delta K_y|$, $Q = \begin{pmatrix} q_x & q_y \\ q_y & q_x \end{pmatrix}$ simplifies to $\begin{pmatrix} 0 & q_y \\ q_y & 0 \end{pmatrix}$ and $\begin{pmatrix} q_x & 0 \\ 0 & q_x \end{pmatrix}$, respectively, so that the vortex topological invariant is

$$\nu = \mathrm{sgn}[\det(Q)] = \begin{cases} -1 & |\Delta K_x| \gg |\Delta K_y| \\ +1 & |\Delta K_x| \ll |\Delta K_y| \end{cases} \tag{B30}$$

Thus, there is vortex phase transition as the WNs "switch partners", i.e., the nearest WN to a given WN changes.

4. Hybridization gap in the continuum limit

Deep in the topological phase, $q_x \ll q_y$, and the eigenvalues of H_{eff} reduce to $\pm|q_y|$. To detect the surface Majorana fermion in this regime, one must thus be at temperatures $T \ll |q_y|/k_B$, which we now estimate.

$|q_y|$, as given by (B29), is straightforward albeit tedious to estimate in the continuum limit $k_x, k_y \ll 1$. Restricting to the $k_z = 0$ plane as done throughout the derivations above, (A3) and (A4), which determine the locations of the WNs, simplify to

$$v_x^2 K_x^2 + v_y^2 K_y^2 = \ell^2 \tag{B31}$$

$$\beta_x K_x^2 + \beta_y K_y^2 = -2m_\Gamma \tag{B32}$$

where $m_\Gamma = m_0 - \sum_{i=x,y,z}\beta_i$. Then, $\hat{M}$, which defines the non-canonical Weyl Hamiltonian H_W'' in (B4) becomes

$$\hat{M} = \begin{pmatrix} v_x^2 K_x/\ell & v_y^2 K_y/\ell \\ \beta_x K_x & \beta_y K_y \end{pmatrix} = R(\phi_\Sigma)\begin{pmatrix} v_X & 0 \\ 0 & v_Y \end{pmatrix} R^T(\phi_p) \tag{B33}$$

Deep in the topological phase of the vortex where $K_y^2 \ll K_x^2$, (B31) implies $\ell \approx K_x v_x$. To ensure consistency with (B32), we must fine-tune $m_\Gamma \approx -\beta_x K_x^2/2$. Note that $|\ell|, |m_\Gamma| \ll |v_x|, |v_y|$ ensures that the WNs occur in the continuum limit, $K_{x,y} \ll 1$. Within the continuum limit, $K_y \ll K_x$ is enforced by fine-tuning β_x without making any of the individual parameters – ℓ, v_x, v_y, β_x, β_y and m_Γ – further small or large in magnitude. In this regime, $\hat{M}$ simplifies to

$$\hat{M} \approx \begin{pmatrix} v_x & v_y^2 K_y/v_x K_x \\ \beta_x K_x & \beta_y K_y \end{pmatrix} = R(\phi_\Sigma)\begin{pmatrix} v_X & 0 \\ 0 & v_Y \end{pmatrix} R^T(\phi_p) \tag{B34}$$

where $v_X, v_Y > 0$, assuming that the singular value decomposition at (K_x, K_y) is achieved by proper rotations. Explicitly,

$$v_X \approx \left| v_x^2 + \beta_x^2 K_x^2 + \frac{(v_y^2/K_x + \beta_x\beta_y K_x)^2}{v_x^2 + \beta_x^2 K_x^2} K_y^2 \right|^{1/2} \approx v_x \tag{B35}$$

$$v_Y \approx \frac{|v_y^2\beta_x/v_x - v_x\beta_y|}{v_x^2 + \beta_x^2 K_x^2} |K_y| \approx \left| \beta_x \frac{v_y^2}{v_x^2} - \beta_y \right| |K_y| \tag{B36}$$

$$|\phi_p| \approx \left| \frac{v_y^2 + \beta_x\beta_y K_x^2}{v_x^2 + \beta_x^2 K_x^2} \frac{K_y}{K_x} \right| \approx \left| \frac{v_y^2 K_y}{v_x^2 K_x} \right| \tag{B37}$$

$$|\phi_\Sigma| \approx \left| \frac{\beta_x^2 K_x^2 + \beta_y^2 K_y^2}{v_x^2 + v_y^4 K_y^2/v_x^2 K_x^2} \right|^{1/2} \approx \left| \frac{\beta_x K_x}{v_x} \right| \tag{B38}$$

Since $v_Y/v_X, |\phi_p| \sim O(K_y/K_x) \ll 1$, this further yields

$$\frac{1}{v_\pm} \approx \pm \frac{1}{v_Y} \tag{B39}$$

$$\mathbb{V}_+ \approx \frac{v_Y}{2\sqrt{2}} \tag{B40}$$

$$\mathbb{V}_- \approx \frac{v_X}{2\sqrt{2}} \tag{B41}$$

$$\frac{\mathbb{V}_+}{\mathbb{V}_-} \approx \frac{v_Y}{v_X} \sim O\left(\frac{K_y}{K_x}\right) \ll 1 \tag{B42}$$

Putting all this together along with $|\phi_\Sigma| \sim O(K_x) \ll 1$ in the continuum limit and $|\theta_d| \approx |v_y K_y / v_x K_x| \ll 1$ deep in the topological phase, we get for $|q_y|$:

$$|q_y| = \frac{1}{4}\beta_y \left(\Delta K_y\right)^2 |\theta_d| \exp\left[-\frac{\xi v_Y \left(\Delta K_y\right)^2}{4\Delta_0} \right] \tag{B43}$$

Assuming typical values for band parameters ($v_Y \sim v_X/10 \sim 10^4 m/s$, $K_y \sim K_x/10 \sim 0.02 \times 2\pi/a$ with $a \approx 6.0$Å, $v_y = v_x$ so that $|\theta_d| \sim 0.1$ and β_y^{-1} ∼bare electron mass) and superconducting properties ($\Delta_0 \sim 5K$ and $\xi \sim 5nm$) gives $|q_y| \sim 0.1K$ and $|q_x| \sim 0$ with $|\Delta K_y \xi| \sim 2 \gtrsim 1$. The vortex originating from individual WNs is $\delta \sim \Delta_0 \hbar v_Y/\mu\xi \sim 1K$ for $\mu \sim 100K$, so that $|q_y| \lesssim \delta \lesssim \Delta_0$, ensuring that we are in the right perturbative regimes. Note that this expression for δ differs from the one that follows from (B18); the latter is only valid at $\mu = 0$ whereas real materials invariable have non-zero $\mu \gg \Delta_0$ and fall in the regime where the former is valid.

Appendix C: Level crossings, Pfaffian and Topological phase transitions

In this section, we select representative points on the phase diagram in Fig. 2 of the main paper, explicitly compare the prediction (Eq. 1 of the main paper) and the result of calculating the Pfaffian-based invariant [4], and show that topological phase transitions are accompanied by level crossings in the vortex as expected. The results are shown in Fig. 2. All the data points in Fig. 2 of the main paper were obtained using the same Pfaffian-based invariant [4].

[1] Liang Fu and C. L. Kane. Superconducting proximity effect and majorana fermions at the surface of a topological insulator. *Physical Review Letters*, 100(9):96407, 2008. ISSN 00319007. doi:10.1103/PhysRevLett.100.096407. URL https://doi.org/10.1103/PhysRevLett.100.096407. B 2

[2] Liang Fu, C L Kane, and E J Mele. Topological Insulators in Three Dimensions. *Physical Review Letters*, 98(10):106803, mar 2007. doi:10.1103/PhysRevLett.98.106803. URL https://link.aps.org/doi/10.1103/PhysRevLett.98.106803. 1

[3] Pavan Hosur, Pouyan Ghaemi, Roger S. K. Mong, and Ashvin Vishwanath. Majorana modes at the ends of superconductor vortices in doped topological insulators. *Physics Review Letters*, 107:097001, Aug 2011. doi:10.1103/PhysRevLett.107.097001. URL https://link.aps.org/doi/10.1103/PhysRevLett.107.097001. B 2

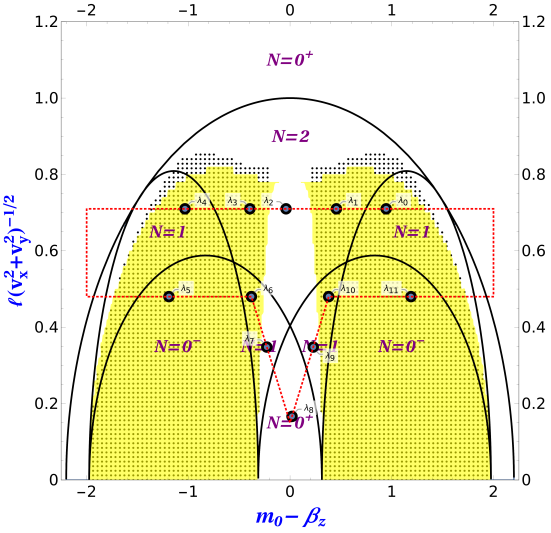

(a)

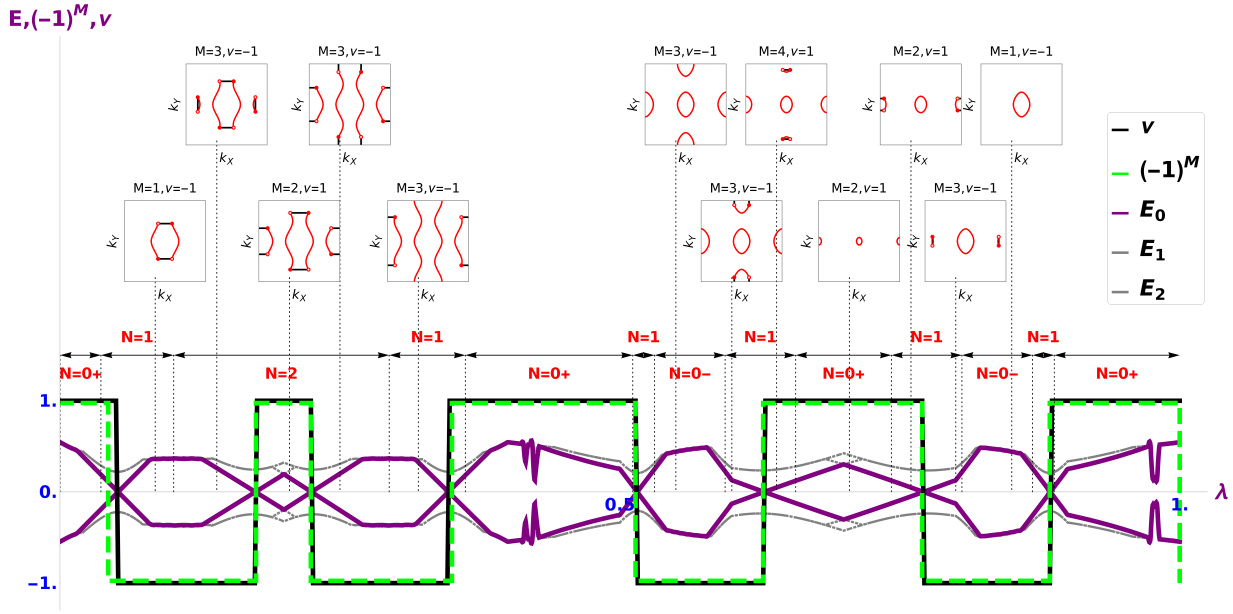

(b)

Figure 2. (a) Representative points and the path for which results are presented in (b). (b) Lowest few energies, predicted topological invariant $(-1)^M$ and the computed invariant ν along the path denoted in (a) parameterized by λ. The insets show the FGSs at each representative point. The predicted and computed results show excellent agreement and each phase transition is accompanied by a level crossing at zero energy.

[4] A Yu Kitaev. Unpaired majorana fermions in quantum wires. *Physics-Uspekhi*, 44(10S):131–136, Oct 2001. doi:10.1070/1063-7869/44/10s/s29. URL https://doi.org/10.10702F1063-78692F442F10s2Fs29. C

[5] N. Read and Dmitry Green. Paired states of fermions in two dimensions with breaking of parity and time-reversal symmetries and the fractional quantum hall effect. *Physical Review B - Condensed Matter and Materials Physics*, 2000. ISSN 1550235X. doi:10.1103/PhysRevB.61.10267. URL https://doi.org/10.1103/PhysRevB.61.10267. B 2